Energy Engineering

Tech Science Press

Doi:10.32604/ee.2025.072787

ARTICLE

Multi-Timescale Flexible Thermal-Electric Coupling Operation of Coal-Fired Thermal Power Units Integrated with Molten Salt Thermal Storage System

Haifeng Li[1], Xiao Li[1], Yuchen Hao[1], Tao Jin[1], Yi Cao[1], Yan Yang[2], Zheng Wang[2], Yuze Zhou[2] and Yao Zou[3,*]

[1]State Grid Jiangsu Electric Power Co., Ltd., Power Dispatching and Control Center, Nanjing, 210024, China
[2]Changzhou Power Supply Company of State Grid Jiangsu Electric Power Co., Ltd., Changzhou, 213000, China
[3]State Key Laboratory of Power Transmission Equipment & System Security and New Technology, Chongqing, 400044, China

*Corresponding Author: Yao Zou. Email: 20183423@cqu.edu.cn

Received: 03 September 2025; Accepted: 28 October 2025; Published: 27 March 2026

ABSTRACT: The increasing penetration of renewable energy sources (RES) imposes stringent flexibility requirements on thermal power units (TPUs). Integrating molten salt thermal storage systems (MSTS) and thermal-electric coupling technologies into TPUs has the potential to improve their operational flexibility and regulation capability. However, existing research seldom investigates the combined effects of MSTS retrofitting and thermal-electric output coupling on short-term dispatchability, especially under rapid load variation conditions. This study proposes a comprehensive modeling and multi-timescale optimization framework for MSTS-retrofitted TPUs with rapid load variation capability, enabling coordinated thermal and electrical dispatch in both day-ahead and real-time stages. The TPU model incorporates steam heating, electric heating, MSTS charge and discharge characteristics, and ladder typer ramping constraints, enabling detailed representation of thermal-electric coupling interactions. The proposed scheduling framework consists of a day-ahead economic dispatch model and a minute-level intraday rolling optimization. In the day-ahead stage, the model maximizes operational revenue while considering flexibility reserve requirements, multi-period peak shaving, reserve allocation, and thermal-electric coupling strategies that coordinate steam and electric heating with MSTS charging and discharging. In the intraday rolling stage, real-time RES fluctuations and load variations are incorporated to update dispatch decisions, ensuring continuous power–heat balance and efficient use of stored thermal energy. Simulation results verify that thermal-electric coupling enhances the system's capability to maintain real-time power balance, while MSTS operation effectively mitigates output fluctuations and supports stable, economical operation for addressing RES variation.

KEYWORDS: Coal-fired thermal power unit; molten salt thermal storage; thermal-electric coupling; multi-timescale operation

1 Introduction

The global pursuit of carbon neutrality has significantly accelerated the deployment of renewable energy sources, with wind and solar power experiencing rapid growth in installed capacity [1]. However, the intrinsic intermittency and volatility of renewable energy sources (RESs), particularly wind power (WP) and photovoltaic (PV) generation, pose substantial challenges to the stability of modern power systems. These fluctuations intensify the demand for flexible resources capable of providing rapid load-following, peak shaving, and frequency regulation services [2].

In regions with limited hydropower potential, retrofitting coal-fired thermal power units (TPUs) to enhance their flexibility has emerged as a viable solution to accommodate variable renewable generation [3]. Such flexibility upgrades primarily include improvements in low-load stable combustion, rapid start-up/shutdown, and fast ramping capabilities [4]. Among them, fast ramping enables real-time adjustment of power output to track load or renewable variability [5]. However, frequent load changes impose considerable thermal and mechanical stress on the system, leading to increased equipment wear and lifecycle degradation. Moreover, operational data indicate that coal consumption during rapid ramping deviates significantly from that during steady-state operation, with efficiency losses in condensate flow and turbine performance resulting in higher fuel usage and more mechanical fatigue [6]. Meanwhile, rapid start-up and shutdown allow units to respond swiftly to dispatch signals or emergency needs, but such frequent cycling also places substantial thermal and mechanical stress on critical components, shortening equipment lifespan and increasing maintenance requirements [7]. To mitigate such impacts and improve ramping performance, molten salt thermal storage (MSTS) retrofits have been introduced to TPUs [8]. By absorbing surplus thermal energy during low-load or high-renewable periods and releasing it during peak demand, the storage system enables rapid electrical output adjustment without frequent thermal cycling of the boiler. However, the flexibility provided by thermal storage alone is often limited by its storage capacity, which restricts its ability to respond to prolonged or large-scale fluctuations. Therefore, a hybrid approach that combines multiple retrofit measures can be developed. By coordinating these strategies, TPUs can dynamically adjust their operation in response to real-time system needs and RES variability, achieving a more balanced trade-off among flexibility, efficiency, and equipment reliability.

However, with the increasing penetration of RES, TPUs are facing growing pressure to enhance their regulation capabilities. It becomes increasingly difficult for TPUs to achieve both wide-range load-following and low coal consumption under rapid ramping conditions. Moreover, the volatility of RESs calls for more precise and responsive adjustments from thermal units within short timescales. These challenges highlight the importance of developing optimized dispatch strategies for TPUs. In [9], a look-ahead economic dispatch model is proposed for wind and thermal power systems, which incorporates tightened ramping constraints for retrofitted TPUs, aiming to mitigate tie-line power fluctuations under high RES penetration. In [10], a coupled dispatch framework is developed for RES and TPUs systems, where ladder-type ramping constraints and flexible reserve constraints are introduced to enhance TPU participation in deep peak regulation.

The above studies primarily focus on optimizing dispatch strategies from the perspective of improving TPU flexibility under rapid load variation. In terms of coordinated scheduling involving TPU and MSTS, several studies have proposed. In [11], a steam-extraction-based TPU retrofitting scheme integrated with MSTS is proposed to enhance low-load flexibility, and a multi-objective grey wolf optimization algorithm is employed to optimize operational parameters and trade-offs between efficiency and ramping performance. In [12], a novel power-to-heat energy storage and power generation system using molten salt is developed to achieve rapid load regulation, with dynamic modeling and exergy analysis revealing its superior ramping capability and potential for control strategy optimization. In [13], a MSTS is embedded in combined heat and power plants (CHPs) to improve load adjustability and reduce coal consumption, and operation scheduling models are developed to quantify flexibility and energy efficiency enhancements. In [14], a multi-stage optimization-based dispatch model is proposed for multi-coupled generation systems integrating TPUs with MSTS retrofitting and rapid load variation capabilities, enabling coordinated peak regulation and improved daily revenue performance. In [15], a three-step decision support method is presented for sizing and optimizing MSTS in CHP plants, demonstrating that retrofitting with storage significantly improves flexibility and long-term economic benefits.

The coupling of power generation and heat supply in TPUs has potential for further improving regulation capability through. The coordinated adjustment of steam heating and electric heating offers additional degrees of freedom for balancing supply and demand in systems with high-RES penetration [16]. In [17], a flexibility retrofit scheme for CHP units integrating internal and external thermal storage is proposed, and a coordinated operation and reserve risk optimization model is developed for a power-heat integrated energy system, demonstrating improved wind accommodation and reserve capacity. In [18], an operation scheduling model for coal-fired CHP stations equipped with electric boilers and heat pumps is established, showing that optimal load allocation among units can reduce coal consumption and CO_2 emissions while improving operational flexibility. In [19], a novel cascade reheat steam extraction system with MSTS is designed for CHP plants, with simulation results indicating enhanced peak shaving capability, higher thermal and exergy efficiency at low loads, and expanded adjustable load ranges.

Although previous studies have explored the integration of MSTS to enhance TPU flexibility, most have focused on relatively long timescale optimization. Few have systematically analyzed how MSTS retrofitting influences TPU flexibility and regulation capability under rapid load variations and multi-timescale operation scenarios. While some works address operation optimization under steady-state or representative scenarios, few consider how TPU flexibility and thermal-electric coupling, i.e., the coordination between thermal and electrical outputs, can be enhanced and fully exploited at shorter time intervals such as minute-level dispatch. However, the thermal-electric coupling significantly increases the dimensionality of the scheduling problem, making real-time optimization more complex than conventional single-energy storage dispatching. These gaps call for a unified optimization framework that captures the dynamic interaction among TPU flexibility, MSTS operation, and thermal-electric coupling across multiple timescales.

To address these limitations, this paper develops a comprehensive modeling and optimization framework for TPUs retrofitted with MSTS and thermal-electric coupling capabilities under multi-timescale scheduling requirements. Unlike general energy-storage-based dispatching models that focus solely on electrical balance, the proposed model simultaneously coordinates both heat and power flows in TPUs integrated with high- and low-temperature MSTS systems. The optimization can satisfy the coupled thermal and electrical equilibrium constraints, where the charging/discharging behavior of the MSTS affects both steam and electrical outputs. The main contributions are as follows:

(1) A detailed TPU model is established that integrates steam heating, electric heating, MSTS retrofitting, and rapid load variation retrofitting, enabling a more accurate representation of operational flexibility and thermal-electric coupling effects.
(2) A multi-timescale scheduling framework is proposed, incorporating both day-ahead optimization and minute-level intraday rolling dispatch, to coordinate TPU flexibility, MSTS operation, and thermal-electric coupling for enhanced system adaptability.
(3) The proposed framework is validated using a real-world power grid case study, the results demonstrate the effectiveness of thermal-electric coupling in improving both day-ahead scheduling efficiency and intraday real-time balancing under RES variations.

2 Operation Model for Thermal Power Unit Considering Molten Salt Thermal Storage Retrofit and Thermal-Electric Coupling

This section presents an operation model for TPUs that integrates a MSTS retrofit and thermal-electric coupling. The model is intended for flexibility retrofit of TPUs operating in power systems with high renewable penetration, aiming to enhance overall system stability and renewable-energy accommodation.

2.1 Operating Characteristics of Thertmal Power Unit after Rapid Load Variation Retrofit

Rapid load variation denotes the ability of a TPU to ramp its output at a significantly higher rate. Achieving this capability requires retrofits in equipment, control systems, and operational strategies. Specifically, optimizing the structure and materials of the boiler and cooling systems reduces thermal inertia and accelerates load-response speed. Advanced control strategies based on artificial intelligence and model predictive control are introduced to improve efficiency under rapid load variation conditions, allowing the unit to ramp quickly and respond promptly to renewable-power fluctuations.

After these retrofits, the unit possesses a rapid ramping capability, its output change rate is markedly increased, enabling swift response to system demand. This capability effectively compensates for the intermittency of wind and solar power, enhancing power-system stability and regulation capacity.

Rapid load variation in TPUs poses major challenges to both control and equipment integrity. When ramping at 2%–3% of rated capacity per minute to follow sharp load or renewable fluctuations, frequent changes in steam pressure and temperature gradients cause thermal fatigue in boiler tubes, creep in turbine blades, and wear in valves and seals. Bearings also experience temperature swings and vibration, reducing their lifespan. Transient mismatches between steam extraction and main flow lead to heat-transfer inefficiency and higher auxiliary power use for feedwater pumps and fans. As a result, the overall efficiency drops during ramping, and maintenance frequency increases. Field tests on subcritical units show efficiency losses of about 0.5–1.5 percentage points and additional degradation costs [20].

2.2 Operation Model of Thertmal Power Unit after Molten Salt Thermal Storage Retrofit and Thermal-Electric Coupling

To overcome the high coal consumption and mechanical wear associated with conventional rapid load variation retrofits, and to meet external heat-supply requirements, thermal-storage retrofitting has become a key flexibility retrofit pathway. The storage system absorbs surplus thermal energy from the TPU and releases it during peak-load periods, improving peak-shaving capability while maintaining rapid load variation on the electrical side. Thermal storage also optimizes unit operation, reducing coal consumption and carbon emissions.

Among storage technologies, molten salt operates stably at high temperatures and is compatible with the high-temperature steam systems of TPUs. Economically, molten-salt materials are low-cost, chemically stable, and long-lasting. Therefore, MSTS-based retrofitting offers clear advantages: thermal efficiency exceeds 90%, and charge/discharge cycles are completed within minutes [21].

The MSTS system comprises storage tanks, heat exchangers, pumps, and piping. Hot and cold tanks form a dual-loop configuration: the high-temperature tank is located between the boiler and the high-pressure turbine cylinder, and the low-temperature tank is located between the turbine working cylinder and the boiler.

Charging occurs during low-load or surplus-generation periods. The high- and low-temperature tanks absorb excess heat from the boiler and turbine working cylinder, respectively, transferring it via heat exchangers to the molten salt, thereby reducing the unit's minimum or surplus output. Discharging occurs during peak-load or renewable-shortfall periods. Stored heat is released: the high-temperature tank increases steam flow to the turbine, while the low-temperature tank preheats feedwater, boosting unit output and heat supply.

After retrofit, the TPU can meet external heat demand through boiler-side steam heat supply P_t^{H} and generator-side electric heat supply P_t^{EH}. Unlike traditional cogeneration units with fixed heat output, molten-salt-retrofitted units realize thermal-electric coupling, meaning that steam and electric heating can be flexibly

coordinated to participate in peak shaving and frequency regulation while mitigating intra-day fluctuations from renewable generation and load variations.

Through charge/discharge of the molten salt storage, the unit can alter boiler-side steam heat supply P_t^{H} and generator-side equivalent electrical output P_t^{TH} without adjusting thermal input P_t^{BURN}, thereby influencing net electrical output P_t^{TPU} and net electric heat supply P_t^{EH}. The retrofitted unit energy-flow diagram is shown in Fig. 1.

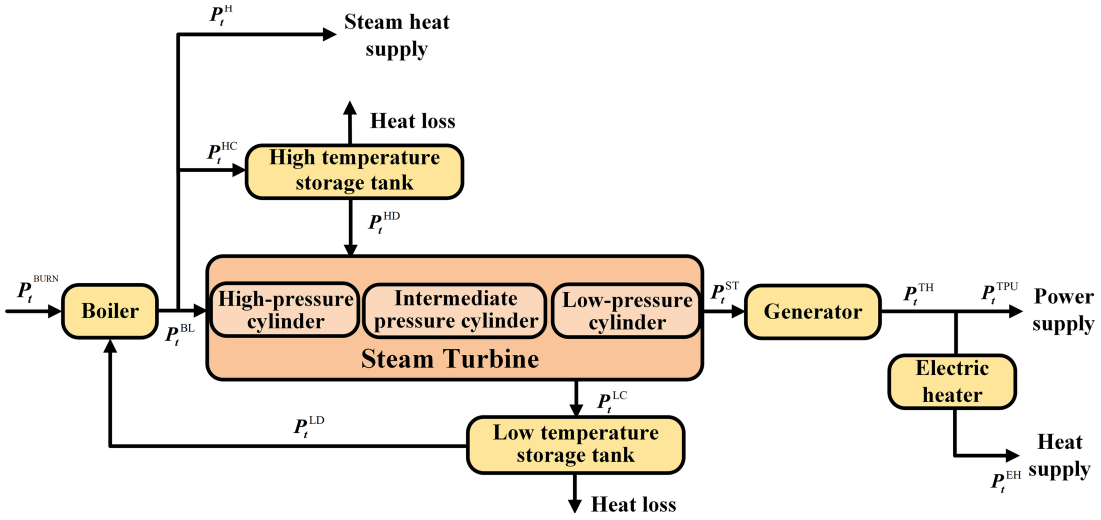

Figure 1: Energy flow diagram of thermal power unit integrated with molten salt thermal storage

In Fig. 1, $P_t^{\mathrm{HC}}/P_t^{\mathrm{HD}}$ and $P_t^{\mathrm{LC}}/P_t^{\mathrm{LD}}$ denote charging/discharging power of the high- and low-temperature storage systems at time t, respectively. P_t^{BL} is the thermal power delivered to the turbine at time t. P_t^{ST} is the thermal power transferred from the turbine to the generator at time t.

When the unit must vary its output to meet electrical and thermal load fluctuations, molten salt storage is used for adjustment. The operating model of the retrofitted unit can be expressed as [14]:

$$\begin{cases} S_t^{\mathrm{H}} = \left(1-\eta^{\mathrm{H}}\right) S_{t-1}^{\mathrm{H}} + \left(\eta^{\mathrm{HC}} P_t^{\mathrm{HC}} - \frac{P_t^{\mathrm{HD}}}{\eta^{\mathrm{HD}}}\right) \Delta t \\ S_t^{\mathrm{L}} = \left(1-\eta^{\mathrm{L}}\right) S_{t-1}^{\mathrm{L}} + \left(\eta^{\mathrm{LC}} P_t^{\mathrm{LC}} - \frac{P_t^{\mathrm{LD}}}{\eta^{\mathrm{LD}}}\right) \Delta t \\ P_t^{\mathrm{BURN}} + P_t^{\mathrm{HD}} - P_t^{\mathrm{HC}} - P_t^{\mathrm{H}} + P_t^{\mathrm{LD}} - P_t^{\mathrm{LC}} = P_t^{\mathrm{ST}} \\ P_t^{\mathrm{BURN}} = \frac{\eta^{\mathrm{coal}} M_t^{\mathrm{coal}} Q_t^{\mathrm{coal}}}{\Delta t} \\ P_t^{\mathrm{TH}} = \eta^{\mathrm{ST}} P_t^{\mathrm{ST}} \\ P_t^{\mathrm{TH}} = P_t^{\mathrm{TPU}} + P_t^{\mathrm{EH}} \end{cases} \tag{1}$$

where S_t^{H}, S_t^{L} are state of charge of the high- and low-temperature storage at time t, respectively. η^{H}, η^{L} are self-discharge rates of the high- and low-temperature storage, respectively. η^{HC}, η^{HD}, η^{LC}, η^{LD} are charging/discharging efficiencies of the high- and low-temperature storage, respectively. η^{coal} is coal combustion efficiency. M_t^{coal} is coal mass consumed at time t; Q_t^{coal} is calorific value of coal; η^{ST} is thermo-electric conversion efficiency.

3 Multi-Time-Scale Coordinated Dispatch Model

This section considers a TPU retrofitted with MSTS and thermal-electric coupling as the research object and develops a multi-timescale coordinated dispatch model. The model is designed to maximize the TPU's integrated daily operational profit through day-ahead and intraday optimal real-time power balance.

3.1 Overall Multi-Timescale Scheduling Framework

The proposed multi-timescale scheduling framework consists of two stages. In the day-ahead optimization, the model takes the predicted net electrical load (difference between total electrical demand and RES generation) and thermal load, as well as their possible fluctuation ranges within a 95% confidence interval, as inputs. The objective is to maximize the overall operational economy of the TPUs with MSTS by determining the optimal 15-min baseline schedules for electrical output, thermal output, and flexibility reserves over a 24-h horizon.

In the intra-day rolling optimization, each 15-min period is used as the scheduling window. A neural network model predicts the minute-level real-time variations of the net load and thermal load, based on which the real-time optimization minimizes the deviations between actual and planned power balance, as well as the deviation from the day-ahead dispatch results. This enables TPUs and MSTS to respond to short-term RES fluctuations while maintaining thermal–electric balance and economic operation.

3.2 Day-Ahead Scheduling Optimization Model

3.2.1 Objective Function

The objective of the day-ahead scheduling optimization model is to maximize the TPUs integrated daily operational profit, denoted as f^{A}

$$\max f^{\mathrm{A}} = \sum_{u \in U} f_u^{\mathrm{TPU}} - f^{\mathrm{RE}} \tag{2}$$

where f_u^{TPU} is the integrated generation profit of the TPU, calculated as

$$f_u^{\mathrm{TPU}} = f_u^{\mathrm{UB}} + f_u^{\mathrm{UD}} - f_u^{\mathrm{UO}} - f_u^{\mathrm{UF}} - f_u^{\mathrm{UE}} - f_u^{\mathrm{UM}} - f_u^{\mathrm{UH}} \tag{3}$$

where f_u^{UB} is the basic electricity-sale revenue. f_u^{UD} is the deep-peak-regulation ancillary-service compensation. f_u^{UO} is the operating cost. f_u^{UF} is the flexibility reserve cost. f_u^{UE} is the pollution-emission cost. f_u^{UM} is the MSTS integrated operating cost. f_u^{UH} is the additional external heat-purchase cost when internal supply is insufficient. Specific formulation are detailed as follows.

(1) RES penalty: When the TPU cannot meet the net load, RES output may be curtailed, and the TPU incurs the associated cost f^{RE} [22]:

$$f_t^{\mathrm{RE}} = \sum_{t=1}^{T} \left[C^{\mathrm{RE,D}} \left(P_t^{\mathrm{WT}*} - P_t^{\mathrm{WT}} + P_t^{\mathrm{PV}*} - P_t^{\mathrm{PV}} \right) \right] \tag{4}$$

where $C^{\mathrm{RE,D}}$ is the RESs (e.g., WP and PV) curtailment cost coefficient. $P_{I,t}^{\mathrm{WT}^*}$, $P_{i,t}^{\mathrm{PV}^*}$ and $P_{i,t}^{\mathrm{WT}}$, $P_{i,t}^{\mathrm{PV}}$ are the maximum-available and actual WP and PV outputs, respectively.

(2) Integrated electricity-sale revenue f_u^{UB} and f_u^{UD}: The comprehensive electricity sales revenue of a TPU can be expressed in the form of the sum of f_u^{UB} and f_u^{UD}. When the generation output is above the

compensation benchmark, only the basic revenue f_u^{UB} applies:

$$f_u^{\mathrm{UB}} = \sum_{t=1}^{T} C_0 P_{u,t}^{\mathrm{TPU}} \tag{5}$$

where, C_0 represents the electricity selling price per unit of base power generation. TPUs can obtain this part of the revenue regardless of their power generation status.

When the unit's generation power is less than the compensation benchmark, in addition to the basic revenue f_u^{UB}, the electricity sales revenue also includes the compensation revenue for participating in peak regulation ancillary services f_u^{UD} [23], expressed as:

$$f_u^{\mathrm{UD}} = \sum_{t=1}^{T} f_{u,t}^{\mathrm{UD}} \tag{6}$$

$$f_{u,t}^{\mathrm{UD}} = \begin{cases} 0 & , \quad \mu_1 < \mu_{u,t}^{\mathrm{TPU}} \le 1 \\ C_1 k_m^{\mathrm{TPU}} \left(\mu_1 P_u^{\mathrm{TPU,max}} - P_{u,t}^{\mathrm{TPU}}\right) & , \quad \mu_2 < \mu_{u,t}^{\mathrm{TPU}} \le \mu_1 \\ C_2 k_m^{\mathrm{TPU}} \left(\mu_1 P_u^{\mathrm{TPU,max}} - P_{u,t}^{\mathrm{TPU}}\right) & , \quad 0 < \mu_{u,t}^{\mathrm{TPU}} \le \mu_2 \end{cases} \tag{7}$$

$$\mu_{u,t}^{\mathrm{TPU}} = \frac{P_{u,t}^{\mathrm{TPU}}}{P_u^{\mathrm{TPU,max}}} \tag{8}$$

where $P_{u,t}^{\mathrm{TPU,max}}$ is the maximum electrical output of the TPUs. C_1 and C_2 are the unit electricity sales prices corresponding to different compensation benchmarks. $\mu_{u,t}^{\mathrm{TPU}}$ is electrical load rate of the TPU. μ_1 and μ_2 are the load rate benchmarks corresponding to the first and second stages of peak regulation compensation, respectively. k_m^{TPU} is the revenue correction coefficient related to the season.

(3) Operational cost of TPUs f_u^{UO}: This cost considers two states, regular peak regulation (RPR) and deep peak regulation (DPR). In the RPR state, the operational cost only considers the unit's power generation coal consumption. In the DPR state, the operational cost includes not only power generation coal consumption but also additional loss costs due to reduced output. f_u^{UO} is calculated as [23]:

$$f_u^{\mathrm{UO}} = \sum_{t=1}^{T} f_{u,t}^{\mathrm{UO}} \tag{9}$$

$$f_{u,t}^{\mathrm{UO}} = \begin{cases} C^{\mathrm{coal}} \left(a^{\mathrm{RPR}} {P_{i,u,t}^{\mathrm{BURN}}}^2 + b^{\mathrm{RPR}} P_{i,u,t}^{\mathrm{BURN}} + c^{\mathrm{RPR}}\right), \\ \mu_1 < \mu_{u,t}^{\mathrm{TPU}} \le 1 \\ C^{\mathrm{coal}} \left(a^{\mathrm{RPR}} {P_{i,u,t}^{\mathrm{BURN}}}^2 + b^{\mathrm{RPR}} P_{i,u,t}^{\mathrm{BURN}} + c^{\mathrm{RPR}}\right) \\ + a^{\mathrm{DPR}} P_{u,t}^{\mathrm{BURN}} + b^{\mathrm{DPR}}, 0 < {\mu_{u,t}}^{\mathrm{TPU}} \le \mu_1 \end{cases} \tag{10}$$

where C^{coal} is the unit price of coal per ton. a^{RPR}, b^{RPR}, and c^{RPR} are the fitting function coefficients for coal consumption of TPU. a^{DPR} and b^{DPR} are the fitting function coefficients for DPR losses.

(4) Flexibility reserve cost of TPUs f_u^{UF}: The flexibility reserve cost of TPUs is calculated as:

$$f_u^{\mathrm{UF}} = \sum_{t=1}^{T} f_{u,t}^{\mathrm{UFU}} + f_{u,t}^{\mathrm{UFD}} \tag{11}$$

where $f_{u,t}^{\mathrm{UFU}}$ and $f_{u,t}^{\mathrm{UFD}}$ are the costs required for providing upward and downward flexibility reserves for the system at time t, respectively. Since the unit's rapid load-following ramp rate upper limit is divided into multiple stages, the flexibility reserve costs vary accordingly at different output stages [24].

(5) Pollutant emission cost of TPU f_u^{UE}: The pollutant emission cost of TPUs is as follows [9]:

$$f_u^{\mathrm{UE}} = \sum_{t=1}^{T} \sum_{h=1}^{H} c_h^{\mathrm{TE}} \frac{\rho_h^{\mathrm{TE}}}{\tau_h^{\mathrm{TE}}} \left(a_h^{\mathrm{TE}} P_{u,t}^{\mathrm{BURN}} + b_h^{\mathrm{TE}} \right). \tag{12}$$

where C_h^{TE}, ρ_h^{TE}, and τ_h^{TE} are the unit treatment cost, emission coefficient per unit of electricity generation, and pollutant conversion coefficient for pollutant h, respectively. a_h^{TE} and b_h^{TE} are the fitting coefficients for pollutant emissions of the TPU, respectively. h is the type of pollutant, H is the total number of pollutants. The pollutants considered in this model are particulate matter (PM), SO_2, and NO_x.

(6) Comprehensive operational cost of MSTS f_u^{UM}: For TPUs retrofitted with MSTS, the internal high/low-temperature incur comprehensive operational costs, including operational and maintenance costs $f_{u,t}^{\mathrm{OB}}$ and life loss costs $f_{u,t}^{\mathrm{LB}}$ [14]:

$$f_u^{\mathrm{UM}} = \sum_{t=1}^{T} \left(f_{u,t}^{\mathrm{OB}} + f_{u,t}^{\mathrm{LB}} \right) \tag{13}$$

During the charging and discharging processes of the MSTS, certain operational and maintenance costs are incurred:

$$f_{u,t}^{\mathrm{OB}} = \mathrm{sum}\left(\left| P_{u,t}^{\mathrm{HD}} + P_{u,t}^{\mathrm{HC}} + P_{u,t}^{\mathrm{LD}} + P_{u,t}^{\mathrm{LC}} \right| \right) C_u^{\mathrm{OB}} \tag{14}$$

where C_u^{OB} is the operation and maintenance cost of the MSTS.

(7) External Heat Purchase Cost of Thermal Power Units f_u^{UM}: TPUs retrofitted with MSTS can export thermal power externally. When the unit cannot meet external heat load demand through steam heating and electric heating, it must purchase heat externally. The external heat purchase cost f_u^{UH} is as follows [25]:

$$f_u^{\mathrm{UH}} = \sum_{t=1}^{T} C_{\mathrm{H,buy}} P_{u,t}^{\mathrm{H,buy}} \tag{15}$$

where $C_{\mathrm{H,buy}}$ is the unit price of external heat purchase. $P_{u,t}^{\mathrm{H,buy}}$ ist the difference between the thermal power exported by the TPU and the external heat load demand.

3.2.2 Constraints

The constraints of the day-ahead scheduling optimization model for thermal and renewable power units can be categorized into power balance, TPU generation constraints, RES constraints, and MSTS constraints.

(1) Power balance constraints: The power balance constraints of this operational model include electrical power balance and thermal power balance.

The electrical power balance constraint requires that the total generation power of TPU and net load (difference between total electrical demand and RES generation) at each time step and under different probability scenarios must meet the load demand:

$$\begin{cases} P_t^{\mathrm{NET}} = \sum_{u=1}^{\mathrm{U}} \left(P_{u,t}^{\mathrm{TH}} - P_{u,t}^{\mathrm{EH}} \right) \\ P_t^{\mathrm{NET}} = P_t^{\mathrm{L}} - P_t^{\mathrm{WT}} - P_t^{\mathrm{PV}} \end{cases} \tag{16}$$

where P_t^{L} is the electrical load demand at time t.

The thermal power balance constraint indicates that TPUs retrofitted with MSTS can meet external heat load demand through steam heating, electric heating, and external heat purchase:

$$P_t^{\mathrm{HL}} = \sum_{u=1}^{\mathrm{U}} \left(\eta^{\mathrm{EH}} P_{u,t}^{\mathrm{EH}} + \eta^{\mathrm{H}} P_{u,t}^{\mathrm{H}} \right) + P_{u,t}^{\mathrm{H,buy}} \tag{17}$$

where P_t^{HL} is the heat load demand at time t. η^{EHS} and η^{H} are the efficiency of EHS and boiler-side steam heat supply.

(2) TPU generation constraints: TPUs generation constraints include unit output upper and lower limits constraints, ramping constraints, and flexibility reserve constraints. First, TPUs must satisfy the output limits and the ladder type ramping rate constraints under rapid load-following conditions [26]:

$$\begin{aligned}
&\forall \mu_{u,t}^{\mathrm{BURN}} \in (\mu_a, \mu_{a+1}), \mu_{u,t}^{\mathrm{BURN,min}} \in (\mu_b, \mu_{b+1}), \mu_{u,t}^{\mathrm{BURN,max}} \in (\mu_c, \mu_{c+1}) \\
&\begin{cases}
P_{u,t}^{\mathrm{BURN}} \le r_c \Delta T + \frac{r_c}{r_a} P_{u,t-1}^{\mathrm{BURN}} - \sum_{x=c}^{a-1} \left(\frac{r_c}{r_{x+1}} - \frac{r_c}{r_x} \right) P_u^{\mathrm{PR},x} \\
P_{u,t}^{\mathrm{BURN}} \ge -r_b \Delta T + \frac{r_b}{r_a} P_{u,t-1}^{\mathrm{BURN}} + \sum_{x=a}^{b-1} \left(\frac{r_b}{r_{x+1}} - \frac{r_b}{r_x} \right) P_u^{\mathrm{PR},x} \\
\sum_{x=c}^{a-1} \left(\frac{r_c}{r_{x+1}} - \frac{r_c}{r_x} \right) P_u^{\mathrm{PR},x} = 0, \forall a = c \\
\sum_{x=a}^{b-1} \left(\frac{r_b}{r_{x+1}} - \frac{r_b}{r_x} \right) P_u^{\mathrm{PR},x} = 0, \forall a = b \\
P_{u,t}^{\mathrm{BURN,min}} \le P_{u,t}^{\mathrm{BURN}} \le P_{u,t}^{\mathrm{BURN,max}}
\end{cases}
\end{aligned} \tag{18}$$

where $\mu_t^{\mathrm{BURN,max}}$ and $\mu_t^{\mathrm{BURN,min}}$ are upper and lower limits of the load rate for the TPUs as calculated in (8) at time t, respectively. μ_a, μ_b, and μ_c are the lower benchmarks of the load rate of TPUs in the peak regulation interval at time t, respectively. $P_u^{\mathrm{PR,x}}$ is the lower limit of the x-th ($x \le X$) output interval. r_x is the upper limit of the ramp rate in the x-th output interval. $P_{u,t}^{\mathrm{BURN,max}}$ and $P_{u,t}^{\mathrm{BURN,min}}$ are upper and lower limits of the TPUs, $P_{u,t}^{\mathrm{BURN,min}} = P_u^{\mathrm{PR},x=X}$.

Second, TPUs must reserve flexibility reserves at each time ΔT to address uncertainties and power imbalances between operational output and load [24]:

$$\begin{cases}
F_{u,t}^{\mathrm{U}} \le \min \left(P_{u,t}^{\mathrm{BURN,max}} - P_{u,t}^{\mathrm{BURN}}, r_c \Delta T + \frac{r_c}{r_a} F_{t-1}^{\mathrm{D},n} - P_{u,t}^{\mathrm{BURN}} - \sum_{x=c}^{a-1} \left(\frac{r_c}{r_{x+1}} - \frac{r_c}{r_x} \right) P_u^{\mathrm{PR},x} \right) \\
F_{u,t}^{\mathrm{D}} \le \min \left(P_{u,t}^{\mathrm{BURN}} - P_2^{\mathrm{PR},n}, r_b \Delta T + P_{u,t}^{\mathrm{BURN}} - \frac{r_b}{r_a} F_{t-1}^{\mathrm{U},n} - \sum_{x=a}^{b-1} \left(\frac{r_b}{r_{x+1}} - \frac{r_b}{r_x} \right) P_u^{\mathrm{PR},x} \right)
\end{cases} \tag{19}$$

where $F_{u,t}^{\mathrm{u}}$ and $F_{u,t}^{\mathrm{D}}$ are the upward and downward flexibility reserves of the TPUs, respectively.

(3) RES generation constraints: When TPU can't meet the power balance, RES can actively reduce part of its output to improve system output stability and operational economy. However, the RES curtaliment in each time step and within one day must not exceed specified limits:

$$\begin{cases}
\mu^{\mathrm{RE}} P_t^{\mathrm{RE,pre}} \le P_t^{\mathrm{RE}} \le P_t^{\mathrm{RE,pre}} \\
\mu^{\mathrm{RE,d}} \sum_{t=1}^{T} P_t^{\mathrm{RE,pre}} \le P_t^{\mathrm{RE}} \le \sum_{t=1}^{T} P_t^{\mathrm{RE,pre}}
\end{cases} \tag{20}$$

where μ^{RE} is the minimum utilization rate of renewable power units; $\mu^{\mathrm{RE,d}}$ is the proportion of the renewable power reduction within one day relative to predicted output; $P_{i,t}^{\mathrm{RE,pre}}$ is the predicted output of renewable power units.

(4) MSTS constraints: The MSTS has capacity constraints and operational constraints [27]. The high/low-temperature constraints are formulated as follows.

$$\begin{cases} S_{\min}^{\mathrm{H}} \le S_t^{\mathrm{H}} \le S_{\max}^{\mathrm{H}} \\ S_{\min}^{\mathrm{L}} \le S_t^{\mathrm{L}} \le S_{\max}^{\mathrm{L}} \end{cases} \tag{21}$$

where $S_{\min}^{\mathrm{H}}$ and $S_{\max}^{\mathrm{H}}$ are the minimum and maximum thermal storage capacity of the high-temperature system at time t, respectively; $S_{\min}^{\mathrm{L}}$ and $S_{\max}^{\mathrm{L}}$ are minimum and maximum thermal storage capacity of the low-temperature system at time t, respectively.
The operational constraints of MSTS are formulated as:

$$\begin{cases} \mu_t^{\mathrm{HD}} + \mu_t^{\mathrm{HC}} \le 1 \\ \mu_t^{\mathrm{LD}} + \mu_t^{\mathrm{LC}} \le 1 \\ \mu_t^{\mathrm{HD}} \le \mu_t^{\mathrm{coal}}, \mu_t^{\mathrm{HC}} \le \mu_t^{\mathrm{coal}} \\ \mu_t^{\mathrm{LD}} \le \mu_t^{\mathrm{coal}}, \mu_t^{\mathrm{LC}} \le \mu_t^{\mathrm{coal}} \\ 0 \le P_t^{\mathrm{HD}} \le \mu_t^{\mathrm{HD}} \theta^{\mathrm{HD}} P_t^{\mathrm{BURN}} \\ 0 \le P_t^{\mathrm{HC}} \le \mu_t^{\mathrm{HC}} P_{\max}^{\mathrm{HC}} \\ 0 \le P_t^{\mathrm{LD}} \le \mu_t^{\mathrm{LD}} \theta^{\mathrm{LD}} P_t^{\mathrm{BURN}} \\ 0 \le P_t^{\mathrm{LC}} \le \mu_t^{\mathrm{LC}} P_{\max}^{\mathrm{LC}} \end{cases} \tag{22}$$

where μ_t^{HD}, μ_t^{HC} and μ_t^{LD}, μ_t^{LC} are the 0–1 variables indicating whether the high/low-temperature thermal storage system is operating, respectively (If in operation, the value is 1; otherwise, it is 0); θ^{HD} and θ^{LD} are maximum heat release coefficients of the high/low-temperature thermal storage systems, respectively; $P_{\max}^{\mathrm{HC}}$ and $P_{\max}^{\mathrm{LC}}$ are the maximum heat release power of the high and low-temperature thermal storage systems, respectively.

(5) Thermal-electric coupling constraints: TPUs retrofitted with MSTS can adjust steam heating and electric heating power through thermal-electric coupling to meet external heat load demand. The steam heating and electric heating power constraints of the TPUs are as follows:

$$\begin{cases} P_{u,t}^{\mathrm{EH,min}} \le P_{u,t}^{\mathrm{EH}} \le P_{u,t}^{\mathrm{EH,max}} \\ 0 \le P_{u,t}^{\mathrm{H}} \le P_{u,t}^{\mathrm{H,max}} \end{cases} \tag{23}$$

where $P_{u,t}^{\mathrm{EH,min}}$ and $P_{u,t}^{\mathrm{EH,max}}$ are the minimum and maximum electric heating power, respectively; $P_u^{\mathrm{H,max}}$, is the maximum steam heating power.

3.3 Intra-Day Rolling Scheduling Optimization Model

Building on the day-ahead scheduling optimization model, this stage incorporates real-time intraday thermal and electrical load data as well as renewable power fluctuations into the optimization process and dispatch strategy. Using the optimal day-ahead schedule at the pre-set time resolution as a reference, an LSTM network is applied to forecast intraday thermal and electrical loads and RES generation [28]. The LSTM approach, which has been widely adopted in power system forecasting, offers high prediction accuracy for capturing short-term variations. Based on these forecasts, a rolling optimization is performed at one-minute intervals within the specified time resolution. The model continuously updates the daily dispatch plan in real time, thereby enabling effective frequency regulation and maintaining power balance.

3.3.1 Objective Function and Constraints

In the intra-day rolling scheduling optimization model, the balance between supply and demand at every single moment is not strictly enforced. The objective function is to minimize, at every temp step, the deviation between generated power and load demand, the deviation between heat supply and heat load, and the deviation between the initial and final intra-day moments and the day-ahead dispatch schedule [29].

$$\min f_{t'}^{\mathrm{RT}} = \sum_{\tau=t'}^{t'+T'} \left(\beta_1 f_\tau^{\mathrm{FE}} + \beta_2 f_\tau^{\mathrm{HE}}\right) + \beta_3 f_\tau^{\mathrm{SE}}, t' = 1, 2, \ldots, T, T' = \Delta t/\Delta t' \tag{24}$$

$$f_\tau^{\mathrm{FE}} = \left| P_\tau^{\mathrm{NET,RT}} - \sum_{u=1}^{\mathrm{U}} \left(P_{u,\tau}^{\mathrm{TH,RT}} - P_{u,\tau}^{\mathrm{EH,RT}}\right) \right| \tag{25}$$

$$f_\tau^{\mathrm{HE}} = \left| P_\tau^{\mathrm{HL,RT}} - \sum_{u=1}^{\mathrm{U}} \left(P_{u,\tau}^{\mathrm{EH,RT}} + P_{u,\tau}^{\mathrm{H,RT}}\right) - P_{u,\tau}^{\mathrm{H,buy,RT}} \right| \tag{26}$$

$$f_\tau^{\mathrm{FE}} = \left| \sum_{u=1}^{\mathrm{U}} \left(P_{u,\tau}^{\mathrm{TH}} - P_{u,\tau}^{\mathrm{EH}}\right) - \sum_{u=1}^{\mathrm{U}} \left(P_{u,\tau}^{\mathrm{TH,RT}} - P_{u,\tau}^{\mathrm{EH,RT}}\right) \right|, \tau = t', t' + T' \tag{27}$$

where Δt is the time interval between $t + 1$ and t, $\Delta t'$ is the time interval between $\tau + 1$ and τ. $f_{\mathrm{t}}^{\mathrm{FE}}$ is the deviation between generated power and net electrical load demand at each real-time dispatch time step τ. f_t^{HE} is the deviation between heat-supply power and heat-load demand at each real-time dispatch moment τ. f^{SE} is the deviation between generated power and the generation schedule at the time steps $\tau = t'$ and $\tau = t' + T'$; β_1, β_2, and β_3 are weighting coefficients for the different objectives.

At each intra-day optimization, the constraints are consistent with the operational constraints of TPUs and MSTS in the day-ahead scheduling model in Section 3.2.2.

3.3.2 Model Linearization

Since the objective function of the intraday rolling optimization model contains absolute-value terms for deviation minimization, the big-M method [30] is adopted in this study for the linearization of absolute-value and logical constraints. This approach is widely applied in mixed-integer linear programming due to its simplicity and generality. However, it may introduce numerical sensitivity if the parameter M is chosen excessively large, leading to ill-conditioned matrices and increased integrality tolerance errors. To ensure stability and accuracy, the value of M is determined through multiple tests.

Taking Eq. (25) as an example, this objective-function component minimizes the deviation between generated power and load demand at each time step. To achieve this, two binary variables, u_τ^{FEP} and u_τ^{FEN}, are introduced to indicate whether the deviation at each real-time dispatch time step τ is positive or negative, respectively. These binary variables satisfy the following relationship:

$$u_\tau^{\mathrm{FEP}} + u_\tau^{\mathrm{FEN}} = 1 \tag{28}$$

After introducing a sufficiently large positive number M, the original objective-function term can be decomposed into:

$$f_\tau^{\mathrm{FE}} = f_\tau^{\mathrm{FEP}} + f_\tau^{\mathrm{FEN}} \tag{29}$$

Then the following constraints are obtained:

$$\begin{cases} f_{\tau}^{\mathrm{FEP}} \geq P_{\tau}^{\mathrm{NET,RT}} - \sum_{u=1}^{\mathrm{U}} \left(P_{u,\tau}^{\mathrm{TH,RT}} - P_{u,\tau}^{\mathrm{EH,RT}}\right) - M\left(1 - u_{\tau}^{\mathrm{FEP}}\right) \\ f_{\tau}^{\mathrm{FEP}} \leq P_{\tau}^{\mathrm{NET,RT}} - \sum_{u=1}^{\mathrm{U}} \left(P_{u,\tau}^{\mathrm{TH,RT}} - P_{u,\tau}^{\mathrm{EH,RT}}\right) + M\left(1 - u_{\tau}^{\mathrm{FEP}}\right) \\ M u_{\tau}^{\mathrm{FEP}} \geq f_{\tau}^{\mathrm{FEP}} \geq 0 \end{cases} \tag{30}$$

$$\begin{cases} f_{\tau}^{\mathrm{FEN}} \geq -\left[P_{\tau}^{\mathrm{NET,RT}} - \sum_{u=1}^{\mathrm{U}} \left(P_{u,\tau}^{\mathrm{TH,RT}} - P_{u,\tau}^{\mathrm{EH,RT}}\right) - M\left(1 - u_{\tau}^{\mathrm{FEN}}\right)\right] \\ f_{\tau}^{\mathrm{FEN}} \leq -\left[P_{\tau}^{\mathrm{NET,RT}} - \sum_{u=1}^{\mathrm{U}} \left(P_{u,\tau}^{\mathrm{TH,RT}} - P_{u,\tau}^{\mathrm{EH,RT}}\right) + M\left(1 - u_{\tau}^{\mathrm{FEN}}\right)\right] \\ M u_{\tau}^{\mathrm{FEN}} \geq f_{\tau}^{\mathrm{FEN}} \geq 0 \end{cases} \tag{31}$$

where f_t^{FEP} and f_t^{FEN} are the positive and negative absolute deviations of generated power and load demand at moment τ, respectively. When the deviation between generated power and load demand is positive, $\mu_{\tau}^{\mathrm{FEP}} = 1$ and $\mu_{\tau}^{\mathrm{FEN}} = 0$, so f_t^{FEP} is positive and f_t^{FEN} is zero. When the deviation is negative, $\mu_{\tau}^{\mathrm{FEP}} = 0$ and $\mu_{\tau}^{\mathrm{FEN}} = 1$, so f_t^{FEP} is zero and f_t^{FEN} is positive. When the deviation is zero, the big-M constraints force the entire value of f_t^{FE} to be zero [31]. Thus, the absolute-value terms in the objective function of the intra-day rolling optimization model can be solved at the minute-by-minute time resolution.

3.4 Solution Method

The proposed day-ahead and intraday optimal dispatch models for MSTS retrofitted TPUs with thermal-electric coupling are implemented in MATLAB, utilizing the YALMIP toolbox as the modeling interface and Gurobi 12.0 as the solver [32].

4 Case Study

4.1 Basic Data

To validate the proposed model, a real-world combined heat and power coal-fired thermal power plant in Jiangsu Province, China, is simulated. The system represents a city-level high-voltage distribution area, where two 600 mw TPUs are located close to the main load centers, supplying electricity and heat to nearby residential and industrial consumers. After retrofitting, the TPUs achieve a minimum output of 30% $P_{u,t}^{\mathrm{BURN,max}}$, with a maximum RPR ramp rate of 1.8 $P_{u,t}^{\mathrm{BURN,max}}$/h, DPR ramp rate 1.2 $P_{u,t}^{\mathrm{BURN,max}}$/h. Meanwhile, the TPUs are equipped with both high- and low-temperature MSTS systems, each providing a maximum charge/discharge power of 100 mw and an energy storage capacity ranging from 30 MWh (minimum) to 300 MWh (maximum). TPUs are equipped with MSTS and incorporate steam heating, adjustable within the range of 0 to 90 mw, and electric heating, adjustable within the range of 40 to 80 mw. The net load of this power plant must accommodate 300 mw of WP and 100 mw of PV. For clarity in presenting the results, the thermal load is converted to MW.

A typical winter day is selected to represent conditions of high thermal demand and high RES output, during which TPUs often experience low net load and deep peak-shaving requirements. This scenario is particularly suitable for evaluating the effectiveness of thermal-electric coupling in ensuring coordinated power and heat supply and enhancing operational stability under high RES variability. The case study adopts a day-ahead scheduling time resolution $\Delta T = 15$ min and an intraday scheduling interval $\Delta T' = 1$ min, with a total scheduling horizon of $T_{\mathrm{s}} = 24$ h $N_{\mathrm{Ts}} = 96$ comprising discrete time intervals. For intraday optimization,

T' = 15 min and rolling optimization is performed every 15 min based on 1-min updates. The simulation utilizes actual operational data, including daily load demand profiles and forecasted PV and wind power generation curves, as illustrated in Fig. 2. Although this study adopts T_s = 24 h, corresponding to the typical time frame used in day-ahead power system scheduling, the proposed model is applicable to any total scheduling horizon by adjusting T_s.

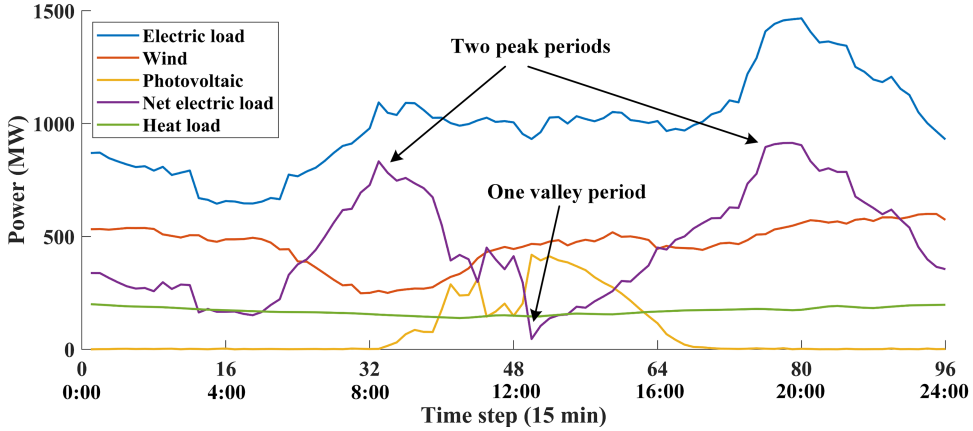

Figure 2: Forecasted load demand and RES (WP/PV) generation profiles

As illustrated in Fig. 2, thermal load demand remains relatively stable throughout the day. Wind power generation exhibits significant fluctuations between 5:15 and 11:00. Electrical load reaches its minimum at 4:00 and peaks at 19:30. The net load of the thermal-storage integrated system drops to its trough at 12:15, primarily due to the high volatility of PV generation between 8:00 and 16:00. This scenario effectively demonstrates the rapid peak-shaving and frequency regulation capabilities of the molten salt thermal energy storage retrofitted thermal power units, leveraging their thermal-electric coupling mechanism.

Other parameters are shown in Table 1. In the table, the deep peak regulation service parameters are adopted from reference [9]. All simulations are executed on a desktop workstation equipped with an AMD Ryzen 7 5700G processor (3.80 GHz base clock) and 16 GB DDR4 RAM.

4.2 Analysis of Day-Ahead Scheduling Optimization Results

Fig. 3 presents the optimized power generation profile of the molten salt thermal energy storage retrofitted thermal power units under 15-min resolution day-ahead scheduling.

As shown in Fig. 3, the system's net load reaches clear valley periods in the early morning (around 4:00) and at midday (around 12:00). During these times, the high- and low-temperature MSTS systems operate in charging mode, with charging power maintained at a relatively high level. This operation enables thermal-electric decoupling, keeping the boiler-side equivalent thermal output stable and preventing a steep rise in coal consumption rates under low-load conditions. At the same time, the electrical output of the TPUs decreases with the drop in net load. Their downward regulation margin, on the order of a few hundred megawatts per unit, provides sufficient negative reserve capacity for the grid, enlarges the downward regulation range of TPUs, and brings notable peak-shaving benefits.

In contrast, during the morning peak (around 8:00) and evening peak (around 20:00), the net load of the thermal-storage system exceeds 1000 mw. The MSTS systems switch to discharging mode, releasing several hundred megawatts of stored thermal energy for power generation. This thermal-electric decoupling effect

keeps fluctuations in coal feed rate relatively small, sustains low operating costs, and allows the units to meet high net load demands while increasing power generation revenue.

Table 1: Basic parameters of case study

Parameter	Value	Parameter	Value
Electricity price under tiered compensation (CNY/MWh)	C_0 = 375, C_1 = 400, C_2 = 800	Heat purchase price (CNY/MWh)	160
Load rate of compensation	μ_1 = 0.5, μ_2 = 0.4	Coal price (CNY/ton)	C^{coal} = 685
Coal consumption coefficients of TPU (ton/MW2, ton/MW, ton)	$a^{\text{RPR}} = 1.69 \times 10^{-5}$, b^{RPR} = 0.276, c^{RPR} = 11.46	Carbon price (CNY/ton)	C_u^{UC} = 85
DPR loss coefficients of TPU (CNY/MWh, CNY)	a^{DPR} = −209.69, b^{DPR} = 87,354.7	Emission treatment cost (CNY/kg)	C_{PM}^{TE} = $C_{SO_2}^{\text{TE}}$ = C_{NOX}^{TE} = 1.2
Revenue correction coefficient of compensation	k_1^{TPU}= k_2^{TPU} = 1	Emission coefficien	ρ_{PM}^{TE} = 3.5, $\rho_{SO_2}^{\text{TE}}$ = 16.3, ρ_{NOX}^{TH} = 40.9
Coefficients for pollutant emissions (kg/MW, kg)	a_h^{TE}= 2935.3, b_h^{TE} = 92,771.2	Pollutant conversion coefficientt	τ_{PM}^{TE} = 2.18, $\tau_{SO_2}^{\text{TE}}$ = 0.95, τ_{NOX}^{TE} = 0.95
Min. utilization rate for RES	μ^{RE} = 0.9	Curtailment cost of RESs (CNY/MWh)	$C^{\text{RE,D}}$ = 1000
Operation and maintenance cost of the MSTS (CNY/MWh)	C_u^{OB} = 80	Self-discharge rates of the MSTS	$\eta^{\text{H}} = \eta^{\text{L}}$ = 0.9996
Charging/discharging efficiencies of the MSTS	$\eta^{\text{HC}} = \eta^{\text{HD}} = \eta^{\text{LC}} = \eta^{\text{LD}}$ = 0.985	Coal combustion efficiency	η^{coal} = 0.89

(Continued)

Table 1 (continued)

Parameter	Value	Parameter	Value
Calorific value of coal (MJ/kg)	$Q_t^{coal} = 29.3$	Thermo-electric conversion efficiency	$\eta^{ST} = 0.99$
Efficiency of EHT	$\eta^{EHS} = 0.55$	Efficiency of boiler-side steam heat supply	$\eta^{H} = 0.9$

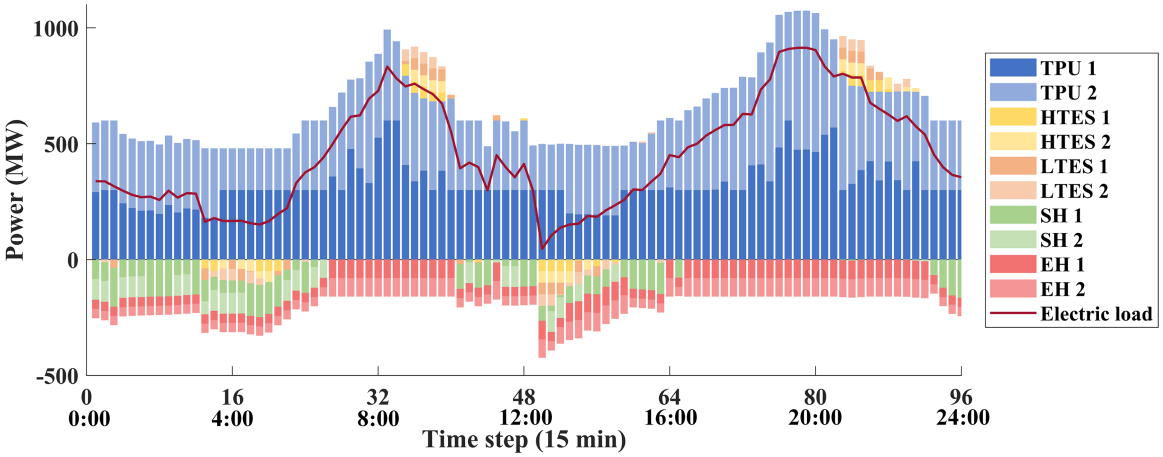

Figure 3: Optimal day-ahead dispatch profile of TPUs with MSTS

To further examine the thermal-electric coupling effects in TPUs, specifically the frequency regulation participation of steam heating and electric heating, Fig. 4 presents the thermal load and heating output curves of the TPUs.

By comparing Fig. 4 with the total output variations in Fig. 3, several operational features are evident. From midnight until early morning, TPUs meet thermal demand entirely through steam and electric heating, without purchasing heat externally, while the MSTS thermal load gradually declines.

During the morning and evening peaks, electric heating output increases while steam heating decreases, with supplementary heat purchased from external sources. This occurs because a higher net electrical load requires greater generator-side output. Under the MSTS power generation effect, steam heating output drops, electric heating rises in parallel with generator output, and power generation revenues offset the cost of external heat procurement, improving TPU profitability.

Around midday, abundant PV output sharply reduces the net load of the thermal storage system. Although boiler-side equivalent thermal output falls markedly compared with the morning peak, it does not fully track the net load minimum because the MSTS is charging at high power. Steam heating output increases while electric heating output declines, and external heat purchases drop to near zero.

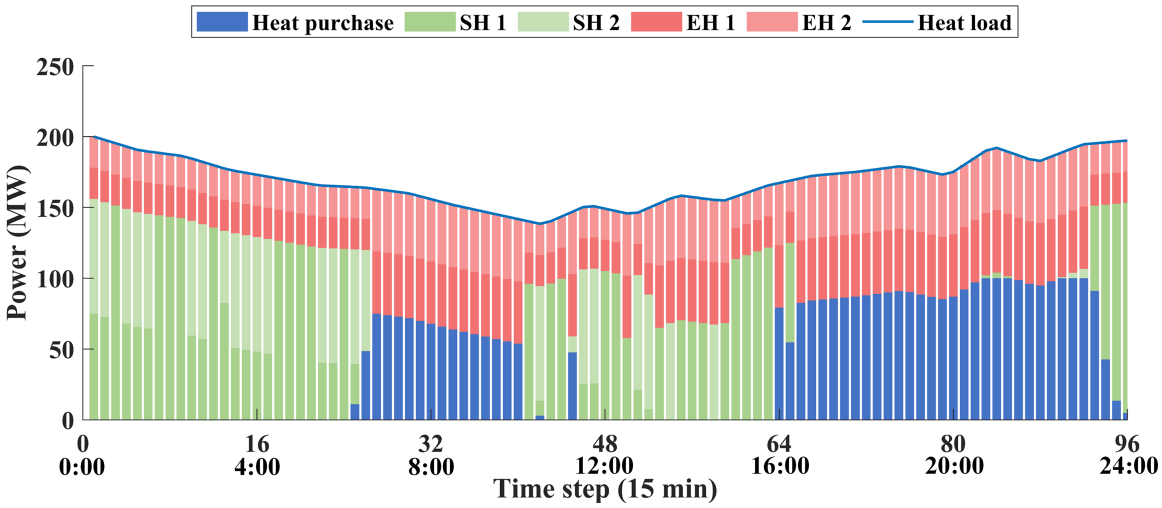

Figure 4: Thermal load and heating output profiles of TPUs with MSTS

Overall, the combination of MSTS-enabled thermal-electric decoupling with the flexible coordination of steam and electric heating enables TPUs to implement "heat-for-power" substitution during net load valleys and "storage-for-coal" substitution during peaks. This strategy extends the units' effective regulation range, limits coal consumption fluctuations on the boiler side, and simultaneously delivers peak-shaving revenues, heating reliability, and operational efficiency.

4.3 Analysis of Intraday Rolling Optimization Results Considering Thermal-Electric Coupling

To comprehensively evaluate the benefits of thermal-electric coupling in MSTS retrofitted TPUs, two operational schemes are compared in this section.

Scheme 1: The TPUs are equipped with MSTS and integrate adjustable steam and electric heating systems with flexible operational ranges as detailed in Section 4.1, both of which actively participate in real-time frequency regulation.

Scheme 2: TPUs are also equipped with MSTS, but both the steam heating and electric heating maintain constant outputs of steam heating at P_t^{H} = 45 mw and electric heating at P_t^{EH} = 40 mw.

Using a one-minute resolution intraday rolling optimization, the comparative power output profiles of Scheme 1 and Scheme 2 are presented in Fig. 5.

Throughout the day, both schemes generally follow the net load trend; however, clear differences emerge under high variability conditions. At around the 720th time step (approximately 12:00 noon), Scheme 2 exhibits a pronounced power imbalance caused by real-time fluctuations in load demand and renewable generation from wind and PV sources. In this fixed-heating-output configuration, steam heating is kept at a constant, leaving no flexibility for compensating sudden changes in net load. As a result, when renewable generation surges, the MSTS-integrated system under Scheme 2 cannot sufficiently reduce its net electrical output, leading to notable overgeneration and consequent curtailment of clean energy. Such unmitigated power deviations also reduce the system's contribution to frequency stability.

In contrast, Scheme 1 enables TPUs equipped with MSTS to flexibly adjust steam heating and electric heating, thereby introducing a highly responsive thermal-electric coupling mechanism. This capability allows the system to offset rapid variations in renewable output and load demand by dynamically reallocating part of the generator's output to heating. As a result, Scheme 1 maintains close alignment with the net load

curve, significantly reducing power deviations. Over the entire day, this operational flexibility improves the system's ability to provide frequency regulation, enhances renewable accommodation, and minimizes wasted generation, thereby increasing the economic return for the plant.

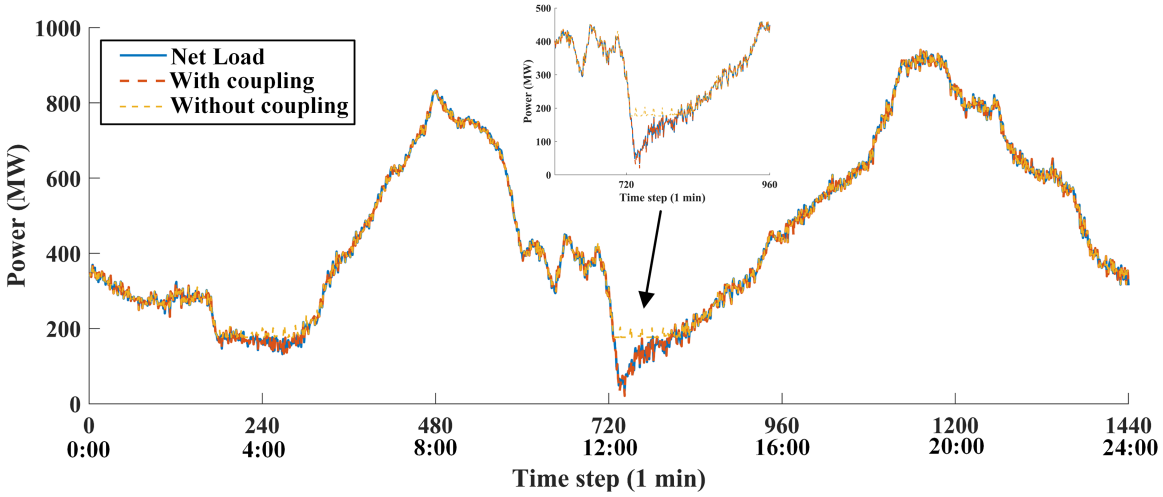

Figure 5: Comparison of total power output profiles for TPUs with MSTS under real-time operational schemes

Fig. 6 presents a magnified view of Scheme 1's output variations between the 600th and 960th time steps, focusing on the behavior before and after the midday net load trough.

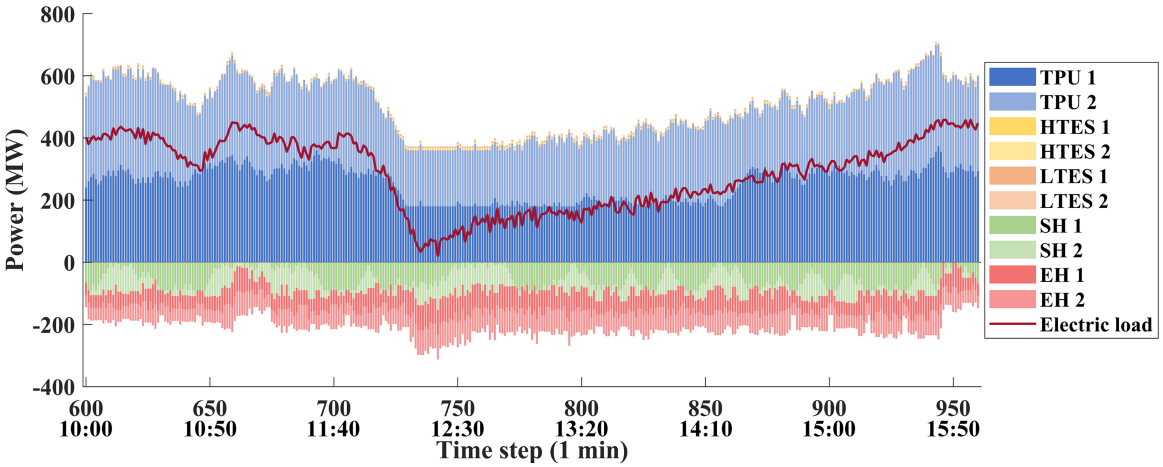

Figure 6: Enlarged view of TPU output variations with thermal-electric coupling for the period around the midday net load trough

Around the 740th time step, the net load of the MSTS-integrated system reaches its lowest point due to a combination of reduced electrical demand and high renewable generation. Under these conditions, the thermal-electric coupling control rapidly increases heating output by raising steam heating and electric heating in coordination, thereby absorbing excess electrical generation capacity that would otherwise lead to overproduction. This coordinated adjustment enables the TPUs to maintain generator output within an optimal range, limiting the ramping rate and avoiding sharp fluctuations in coal feed rate at the boiler side. The ability to flexibly convert excess electrical output into thermal energy also ensures that the stored

thermal energy can be later used during peak demand periods, improving both operational stability and economic performance.

By contrast, when thermal-electric coupling is absent and heating outputs are fixed, the MSTS primarily serves its long-term energy-shifting role, with minimal effect on short-term frequency regulation or rapid load fluctuation suppression. This limitation is evident in the larger deviations from the net load curve in Scheme 2. Overall, the results in Fig. 6 demonstrate that integrating thermal-electric coupling into TPUs with MSTS not only expands their short-term regulation capability but also enhances system resilience against rapid intraday variability.

Table 2 compares the key operational outcomes under the thermal–electric coupling and non-coupling schemes. As shown, the coupling scheme achieves a 5.56% increase in total revenue, demonstrating improved economic performance through flexible coordination between heat and power outputs. Meanwhile, the total power supply–demand imbalance is reduced by 92.78%, indicating that the proposed thermoelectric coupling control enables more accurate real-time regulation and enhances system stability. The total purchased heat rises by only 6.38%, reflecting a moderate trade-off between external heat procurement and additional power generation income. These results verify that the proposed coupling strategy substantially improves renewable accommodation, operational stability, and economic benefits compared with conventional operation without thermal–electric coupling.

Table 2: Comparison of key results between thermal–electric coupling and non-coupling schemes

Parameter	Total revenue (CNY)	Total power supply–demand imbalance (MWh)	Total purchased heat (MWh)
Thermal–electric coupling (Scheme 1)	1.4042×10^7	129.7	1068.1
Non-coupling (Scheme 2)	1.3303×10^7	9.37	999.9

5 Conclusion and Future Work

This paper proposes a thermal-electric coupling control strategy for MSTS-retrofitted TPUs, aiming to enhance their short-term regulation capability and operational economy under high renewable penetration. The strategy enables flexible adjustment of both steam heating and electric heating outputs in real time, thereby coupling thermal and electrical outputs for improved system flexibility. While addressing the above challenges, a day-ahead scheduling model with 15-min resolution and an intraday rolling optimization with 1-min resolution are developed. The day-ahead scheduling considers optimal coordination of power generation, thermal supply, and MSTS charging/discharging to maximize economic benefits and ensure heating reliability over a 24-h horizon. The intraday rolling optimization focuses on real-time adjustment of steam heating and electric heating outputs in response to minute-level variations in net load and renewable generation, aiming to improve frequency regulation performance and mitigate short-term power fluctuations. Simulation results show that the thermal-electric coupling scheme effectively smooths short-term power fluctuations, reduces overgeneration during renewable surges, and enhances the utilization of MSTS for frequency regulation. In day-ahead scheduling, it broadens the TPUs' regulation range, maintains stable boiler-side coal feed rates, and achieves both peak-shaving revenue and heating reliability. At the minute-level timescale, it demonstrates superior responsiveness to real-time net load variations by

reallocating generator output to heating, significantly reducing power deviations compared to the fixed-heating scheme. Overall, the proposed strategy enhances renewable accommodation, operational stability, and economic returns, as evidenced by the quantitative results showing a 5.56% increase in total revenue and a 92.78% reduction in supply–demand imbalance under the coupling scheme, offering a practical pathway for upgrading TPUs to meet the flexibility requirements of modern power systems.

In future research, the proposed multi-timescale thermoelectric coupling scheduling framework can be extended to incorporate risk-aware optimization techniques to handle renewable and load uncertainties more comprehensively. Approaches such as the risk-factor-oriented stochastic dominance method [33] can quantify and manage multi-source operational risks, enabling TPUs with MSTS to make adaptive decisions under uncertain power and heat demands. Moreover, combining physical flexibility from MSTS with financial flexibility from energy markets will further enhance the resilience and economic efficiency of the system.

Acknowledgement: Not applicable.

Funding Statement: This research was funded by State Grid Jiangsu Electric Power Co., Ltd. Science and Technology Project, grant number J2023118.

Author Contributions: The authors confirm contribution to the paper as follows: Study conception and design, Haifeng Li, Yan Yang and Yao Zou; data collection, Xiao Li, Yuchen Hao, Tao Jin, Yi Cao, Zheng Wang and Yuze Zhou; analysis and interpretation of results, Haifeng Li, Xiao Li, Yuchen Hao, Yan Yang, Zheng Wang and Yao Zou; draft manuscript preparation, Tao Jin, Yi Cao, Yuze Zhou and Yao Zou. All authors reviewed the results and approved the final version of the manuscript.

Availability of Data and Materials: Data not available due to commercial restrictions.

Ethics Approval: Not applicable.

Conflicts of Interest: The authors declare no conflicts of interest to report regarding the present study.

References

1. Yu B, Fang D, Xiao K, Pan Y. Drivers of renewable energy penetration and its role in power sector's deep decarbonization towards carbon peak. Renew Sustain Energy Rev. 2023;178:113247. doi:10.1016/j.rser.2023.113247.
2. Mladenov V, Chobanov V, Georgiev A. Impact of renewable energy sources on power system flexibility requirements. Energies. 2021;14:2813. doi:10.3390/en14102813.
3. Hu W, Sun R, Zhang K, Liu M, Yan J. Thermoeconomic analysis and multiple parameter optimization of a combined heat and power plant based on molten salt heat storage. J Energy Storage. 2023;72:108698. doi:10.1016/j.est.2023.108698.
4. Cui RY, Hultman N, Cui D, McJeon H, Yu S, Edwards MR, et al. A plant-by-plant strategy for high-ambition coal power phaseout in China. Nat Commun. 2021;12:1468. doi:10.1038/s41467-021-21786-0.
5. Jiang J, Zhu Y, Wang Y, Guo X, Lv J, Qin J, et al. Unit commitment with bidirectional ramping constraints of flexibility retrofit thermal power unit. Int J Electr Power Energy Syst. 2025;168:110709. doi:10.1016/j.ijepes.2025.110709.
6. Wang C, Liu M, Li B, Liu Y, Yan J. Thermodynamic analysis on the transient cycling of coal-fired power plants: simulation study of a 660 MW supercritical unit. Energy. 2017;122:505–27. doi:10.1016/j.energy.2017.01.123.
7. Miao L, Liu M, Zhang K, Yan J. Design and performance evaluation of thermal energy storage system with hybrid heat sources integrated within a coal-fired power plant. J Energy Storage. 2024;82:110611. doi:10.1016/j.est.2024.110611.

8. Liu X, Zhang L, Jin K, Xue X, Zhou H. Integration model and performance analysis of coupled thermal energy storage and ejector flexibility retrofit for 600 MW thermal power units. J Clean Prod. 2023;428:139337. doi:10.1016/j.jclepro.2023.139337.
9. Yang L, Zhou N, Zhou G, Chi Y, Chen N, Wang L. Day-ahead optimal dispatch model for coupled system considering ladder-type ramping rate and flexible spinning reserve of thermal power units. J Mod Power Syst Clean Energy. 2022;10(6):1482–93. doi:10.35833/MPCE.2021.000801.
10. Lei C, Bu S, Wang Q, Chen Q, Yang L, Chi Y. Look-ahead rolling economic dispatch approach for wind-thermal-bundled power system considering dynamic ramping and flexible load transfer strategy. IEEE Trans Power Syst. 2024;39(1):186–202. doi:10.1109/TPWRS.2023.3238035.
11. Li B, Cao Y, He T, Si F. Thermodynamic analysis and operation strategy optimization of coupled molten salt energy storage system for coal-fired power plant. Appl Therm Eng. 2024;236:121702. doi:10.1016/j.applthermaleng.2023.121702.
12. Hu W, Liu M, Zhang J, Zhang S, Yan J. Load cycling rate of power-to-heat molten salt thermal storage and power generation system: dynamic modeling and performance evaluation. J Energy Storage. 2025;125:116982. doi:10.1016/j.est.2025.116982.
13. Tang H, Liu M, Zhang K, Zhang S, Wang C, Yan J. Performance evaluation and operation optimization of a combined heat and power plant integrated with molten salt heat storage system. Appl Therm Eng. 2024;245:122848. doi:10.1016/j.applthermaleng.2024.122848.
14. Zhou N, Xu Z, Chi Y, Zou Y, Xu F, Dai X. Optimal dispatch of multi-coupling systems considering molten salt thermal energy storage retrofit and cost allocation under rapid load variations. Appl Sci. 2025;15:4062. doi:10.3390/app15074062.
15. Benalcazar P. Sizing and optimizing the operation of thermal energy storage units in combined heat and power plants: an integrated modeling approach. Energy Convers Manage. 2021;242:114255. doi:10.1016/j.enconman.2021.114255.
16. Zhu K, Zhang G, Zhu C, Niu Y, Liu J. A bi-level optimization strategy for flexible and economic operation of the CHP units based on reinforcement learning and multi-objective MPC. Appl Energy. 2025;391:125850. doi:10.1016/j.apenergy.2025.125850.
17. Guo X, Lou S, Chen Z, Wu Y, Wang Y. Stochastic optimal scheduling considering reserve characteristics of retrofitted combined heat and power plants. Int J Electr Power Energy Syst. 2022;140:108051. doi:10.1016/j.ijepes.2022.108051.
18. Liu M, Wang S, Yan J. Operation scheduling of a coal-fired CHP station integrated with power-to-heat devices with detail CHP unit models by particle swarm optimization algorithm. Energy. 2020;204:119022. doi:10.1016/j.energy.2020.119022.
19. Chen C, Ge Z, Zhang Y. Study of combined heat and power plant integration with thermal energy storage for operational flexibility. Appl Therm Eng. 2023;219:119537. doi:10.1016/j.applthermaleng.2022.119537.
20. Wang C, Chen F, Xu P, Cao H, Wang W, Sun Q. Dynamic simulation of a subcritical coal-fired power plant with the emphasis on flexibility. Appl Energy. 2025;392:125976. doi:10.1016/j.apenergy.2025.125976.
21. Zhang P, Ma F, Xiao X. Thermal energy storage and retrieval characteristics of a molten-salt latent heat thermal energy storage system. Appl Energy. 2016;173:255–71. doi:10.1016/j.apenergy.2016.04.012.
22. Zhong J, Li Y, Wu Y, Cao Y, Li Z, Peng Y, et al. Optimal operation of energy hub: an integrated model combined distributionally robust optimization method with Stackelberg game. IEEE Trans Sustain Energy. 2023;14(3):1835–48. doi:10.1109/TSTE.2023.3252519.
23. Zou Y, Wang Q, Xia Q, Chi Y, Lei C, Zhou N. Federated reinforcement learning for short-time scale operation of wind-solar-thermal power network with nonconvex models. Int J Electr Power Energy Syst. 2024;158:109980. doi:10.1016/j.ijepes.2024.109980.
24. Wang C, Song J, You D, Zheng W, Guo J, Zhu L. Combined heat and power plants integrated with steam turbine renovations: optimal dispatch for maximizing the consumption of renewable energy. Energ Convers Manage. 2022;258:115561. doi:10.1016/j.enconman.2022.115561.

25. Li Z, Wu L, Xu Y, Zheng X. Building microgrid considering practical thermal loads and battery degradation. IEEE Trans Sustain Energy. 2022;13(2):668–82. doi:10.1109/TSTE.2021.3126776.
26. Yang L, Zhou N, Zhou G, Chi Y, Wang Q, Lyu X, et al. An accurate ladder-type ramp rate constraint derived from field test data for thermal power unit with deep peak regulation. IEEE Trans Power Syst. 2024;39(1):1408–20. doi:10.1109/TPWRS.2023.3241208.
27. Xu J, Liu W, Lv K, Wang Z, Ma S, Zhao G, et al. Comparative investigation on the thermodynamic performance of coal-fired power plant integrating with the molten salt thermal storage system. J Energy Storage. 2024;89:111738. doi:10.1016/j.est.2024.111738.
28. Xia M, Shao H, Ma X, de Silva CW. A stacked GRU-RNN-based approach for predicting renewable energy and electricity load for smart grid operation. IEEE Trans Ind Inform. 2021;17(10):7050–9. doi:10.1109/TII.2021.3056867.
29. Ma X, Peng B, Ma X, Tian C, Yan Y. Multi-timescale optimization scheduling of regional integrated energy system based on source-load joint forecasting. Energy. 2023;283:129186. doi:10.1016/j.energy.2023.129186.
30. Zhou Y, Wang Q, Chicco G, Liao J, Chi Y, Huang T, et al. Dynamic decoupling-based convex-concave programming for optimal power flow in asymmetric bipolar DC distribution networks. IEEE Trans Power Syst. 2025;40(3):2376–88. doi:10.1109/TPWRS.2024.3496752.
31. Lei C, Wang Q, Zhou G, Bu S, Zhou N, Lin T, et al. Probabilistic wind power expansion planning of bundled wind-thermal generation system with retrofitted coal-fired plants using load transfer optimization. Int J Electr Power Energy Syst. 2023;151:109145. doi:10.1016/j.ijepes.2023.109145.
32. Gurobi Optimization LLC. Gurobi optimizer [Internet]. Beaverton, OR, USA: Gurobi Optimization; 2025 [cited 2025 Aug 9]. Available from: https://www.gurobi.com/.
33. Xiao D, Lin Z, Wu Q, Meng A, Yin H, Lin Z. Risk-factor-oriented stochastic dominance approach for industrial integrated energy system operation leveraging physical and financial flexible resources. Appl Energy. 2025;377:124347. doi:10.1016/j.apenergy.2024.124347.